Kawabata *et al.*
Progress in Earth and Planetary Science (2023) 10:28
https://doi.org/10.1186/s40645-023-00557-z

Progress in Earth and Planetary Science

RESEARCH ARTICLE

Open Access

Relationship between strain accumulation and release associated with recent slow slip events on the Japanese Islands

Hiroki Kawabata[1*], Shoichi Yoshioka[1,2] and Francisco Ortega-Culaciati[3]

Abstract

In this study, we investigated the relationship between the strain accumulation before a slow slip event (SSE) and the strain release during the SSE for three recent SSEs along the Suruga Trough, Sagami Trough, and Nankai Trough, which are subduction zones in central to southwest Japan. The three analysed SSEs were the 2013–2016 Tokai long-term SSE (L-SSE), the 2018 Boso-Oki short-term SSE (S-SSE), and the 2019–2021 Central Shikoku L-SSE. We applied exponential and logarithmic functions to remove the postseismic deformations caused by the Mw 9.0 2011 Tohoku-Oki earthquake. We discovered a strong negative correlation between strain accumulation and strain release in the dilatation of all three SSEs and in the maximum shear strain of the 2018 Boso-Oki S-SSE. A comparison of the amount of strain accumulation with that of strain release revealed that approximately 30% of the strain was released in the 2013–2016 Tokai L-SSE, that 40% of the strain was released in the 2019–2021 Central Shikoku L-SSE, and that approximately 60% of the strain was released in the 2018 Boso-Oki S-SSE. This finding suggests that all of the accumulated strains are not necessarily released by the SSEs.

Keywords GNSS, Slow slip event, Strain accumulation and release, Tokai region, Boso-Oki, Shikoku region, Subduction zone

1 Introduction

In many subduction zones in and around the Japanese Islands, slow slip events (SSEs) and aseismic interplate slip events with long durations that are different from regular earthquakes occur every few years. Slow slip events can be categorized into two groups: long-term slow slip events (L-SSEs) with durations of several months to a couple of years and short-term slow slip events (S-SSEs) with durations of several days to a couple of weeks. In and around the southwestern Japanese Islands, L-SSEs mainly occur at the plate boundary between the oceanic Philippine Sea plate and the continental Amurian plate and have been frequently observed in the Bungo Channel (e.g. Ozawa et al. 2013; Yoshioka et al. 2015; Seshimo and Yoshioka 2022), Kii Channel (e.g. Kobayashi 2017), Tokai region (e.g. Ozawa et al. 2002), and Shikoku region (e.g. Kobayashi 2010) (Fig. 1). S-SSEs are anticipated off the Boso Peninsula along the Sagami Trough, which is a subduction zone between the Philippine Sea plate and the continental North American plate (e.g. Ozawa et al. 2007) (Fig. 1).

Kawabata and Yoshioka (2023) employed the Global Navigation Satellite System (GNSS) to investigate the relationship between the accumulation of strain and the release of strain before and after the SSE for the Tokai L-SSE in 2000–2005, the Bungo Channel L-SSEs in 2009–2010 and 2018–2019, and the Boso-Oki S-SSE in 2007.

*Correspondence:
Hiroki Kawabata
222s410s@gsuite.kobe-u.ac.jp
[1] Department of Planetology, Graduate School of Science, Kobe University, Rokkodai-cho 1-1, Nada ward, Kobe 657-8501, Japan
[2] Research Center for Urban Safety and Security, Kobe University, Rokkodai-cho 1-1, Nada ward, Kobe 657-8501, Japan
[3] Department of Geophysics, Faculty of Physical and Mathematical Sciences, University of Chile, Av. Blanco Encalada 2002, Santiago, Chile

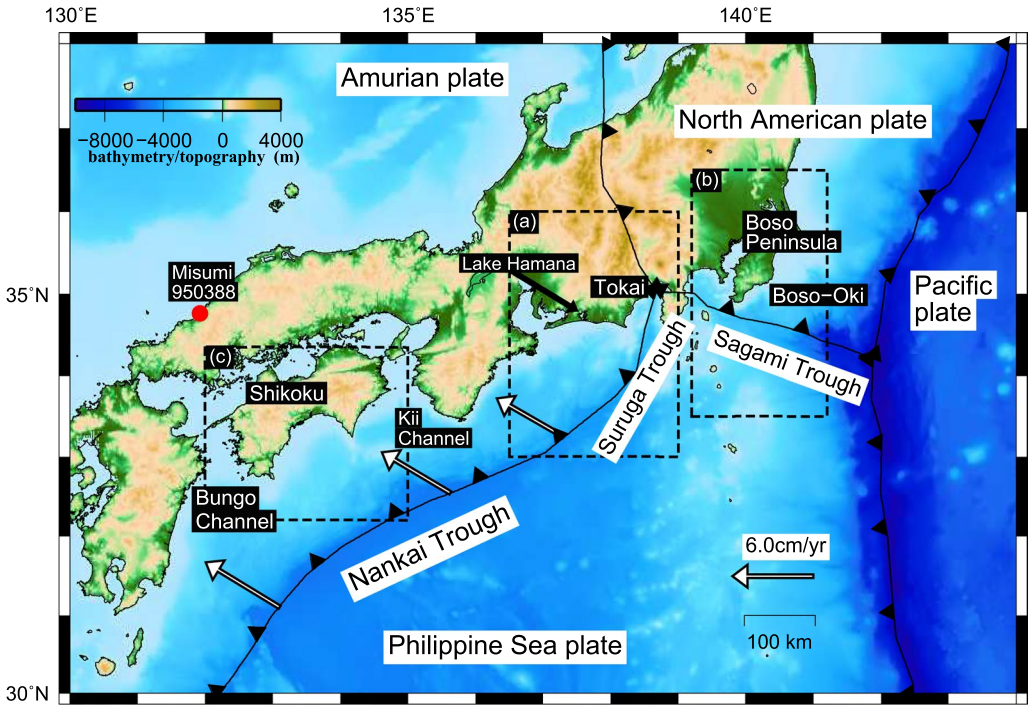

Fig. 1 Tectonic map of central to southwest Japan. The solid black lines represent the plate boundaries (Bird 2003), and the black triangles point in the direction of the motion of the subducted plate. The white arrows represent plate motion velocity vectors of the Philippine Sea plate with respect to the Amurian plate (DeMets et al. 2010). The red circle represents the GNSS station that serves as a reference station (Misumi). The three regions enclosed by dashed rectangles are the areas analysed in this study, which are shown in Fig. 2

One of the features of SSEs is that they have much shorter recurrence intervals than megathrust earthquakes. Since the time of the previous SSE in each occurrence region is known, the period of strain accumulation can be clearly identified. Using the same method by Kawabata and Yoshioka (2023), we report the results of the relationship between the accumulation of strain before the SSE and the release of strain at the time of the SSE for three recent SSEs—the Tokai L-SSE (1 January 2013–5 February 2016), Boso-Oki S-SSE (5 June 2018–20 June 2018), and Central Shikoku L-SSE (1 January 2019–31 December 2021)—which occurred in different regions.

2 Methods/experimental

The applied data consisted of the F5 solution of the daily coordinate positioning values provided by the Geospatial Information Authority of Japan (GSI). The distribution of the GNSS stations utilized in the analysis of each SSE is shown in Fig. 2a–c. The reference station was set as the Misumi station (950388) for all of our analyses (Fig. 1). In this study, the east–west and north–south components of horizontal displacements were applied. The number of GNSS observation stations utilized in the analysis of each SSE and the analysis periods before and during the SSEs are shown in Table 1. For the preoccurrence period, the analysis start date for strain accumulation was the first day after the end of the previous SSE.

2.1 Data processing of time series data

In this section, we present the procedure for analysing GNSS time series data. We followed the analysis method of Seshimo and Yoshioka (2022). First, we corrected for steps due to antenna exchange in the GNSS time series data. This correction was performed by taking the difference between the averages of the 10 days before and after the date of antenna exchange at each GNSS station when a step of 1 cm or more was observed on the date of antenna exchange. Second, the coseismic steps were corrected in the same way, and the following curve fitting equation was applied to the time series data for the period when no SSEs occurred.

$$y(t) = a + bt + c\sin\left(\frac{2\pi t}{T}\right) + d\cos\left(\frac{2\pi t}{T}\right) + e\sin\left(\frac{4\pi t}{T}\right) + f\cos\left(\frac{4\pi t}{T}\right) \quad (1)$$

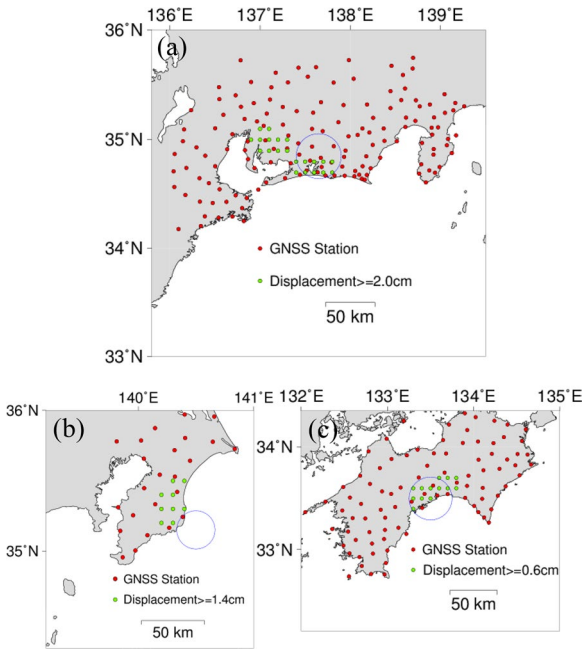

Fig. 2 Spatial distributions of the GNSS stations employed in this study. The red dots denote the GNSS stations selected for our analysis. The green dots represent the calculation points whose displacement exceeded the threshold shown in each figure at the time of the SSE. The blue circles indicate the approximate location of each SSE. **a** 2013–2016 Tokai L-SSE, **b** 2018 Boso-Oki S-SSE, and **c** 2019–2021 Central Shikoku L-SSE

where t is the time elapsed from the analysis start date, $y(t)$ is the approximate curve, and T is one year. The unknown coefficients a, b, c, d, e and f for each term were determined by the least squares method. The first and second terms on the right-hand side represent the linear trend of the steady-state crustal deformation, and the third to sixth terms on the right-hand side represent the annual and semiannual variations. For the three SSEs, the estimated periods of the linear trends of the steady-state crustal deformations are tabulated in Table 2. The approximate curves obtained by the above method were then subtracted from the GNSS time series data.

Third, we removed the postseismic deformation caused by the Tohoku-Oki earthquake (Mw 9.0 on 11 March 2011). All of the SSEs targeted in this study occurred after this massive earthquake and were strongly affected by postseismic deformation, especially in the Boso Peninsula and Tokai region. Therefore, the effects of postseismic deformation that were associated with the 2011 Tohoku-Oki earthquake needed to be removed from GNSS time series data, which was performed using the method proposed by Tobita (2016) and Ozawa et al. (2016). Curve fitting of the postseismic deformation was performed for the 2019–2021 Central Shikoku L-SSE and the 2018 Boso-Oki S-SSE using the following equation:

$$Y(t) = A \ln\left(1 + \frac{t-t_0}{t_1}\right) + B \ln\left(1 + \frac{t-t_0}{t_2}\right) + C \exp\left(\frac{-(t-t_0)}{t_3}\right) + D \quad (2)$$

where t is the elapsed time from the analysis start date, namely, 1 January 2011, and the estimated period for the postseismic deformation was from 12 March 2011 to 31 December 2014. $Y(t)$ is the approximate curve, and t_0 is the date of occurrence of the Tohoku-Oki earthquake. The terms on the right-hand side represent the postseismic deformation. t_1, t_2, and t_3 were the time constants, whose values were obtained from Tobita (2016). The unknown coefficients A, B, C and D for each component were determined by the least squares method. For the two SSEs mentioned above, postseismic deformation was estimated using data for the period from the occurrence of the Tohoku-Oki earthquake to the end of 2014. However, as the Tokai L-SSE occurred in 2013, and postseismic deformation could not be estimated using data from the above period. If the estimation period was shortened, it would not possible to fit the data well. Since the curve fitting could not be adequately performed with Eq. (2), for the 2013–2016 Tokai L-SSE, the following equation

Table 2 Estimated periods of the linear trends of the steady-state crustal deformations

SSE	Estimated period
Tokai L-SSE	1 January 2006–31 December 2007
Boso-Oki S-SSE	1 January 2008–31 December 2009
Central Shikoku L-SSE	1 January 2016–31 December 2017

Table 1 Analysis period before and during the occurrence of each SSE

SSE	Number of observation stations	Analysis period prior to the SSE (years)	Analysis period during the SSE occurrence (years)
Tokai L-SSE	146	1 July 2005–31 December 2012 (7.5)	1 January 2013–5 February 2016 (3.1)
Boso-Oki S-SSE	24	10 January 2014–4 June 2018 (4.4)	5 June 2018–20 June 2018 (0.04)
Central Shikoku L-SSE	87	1 January 2014–31 December 2018 (5.0)	1 January 2019–31 December 2021 (3.0)

by Ozawa et al. (2016) was applied to perform curve fitting for the postseismic deformation.

$$Y(t) = A \ln\left(1 + \frac{t-t_0}{t_1}\right) + B\left(\exp\left(\frac{-(t-t_0)}{t_2}\right) - 1\right) + C \tag{3}$$

The meaning of each variable is the same as that in Eq. (2). The estimation period of the postseismic deformation is from 12 March 2011 to 11 October 2012. For the 2013–2016 Tokai L-SSE only, the estimated period of the postseismic deformation was different. The curves obtained from Eqs. (2) and (3) were used to extract the steady-state crustal deformation before the SSE and the crustal deformation caused by the SSE. The postseismic deformation components obtained from Eqs. (2) and (3) were removed from the time series data before and during the occurrence of the SSEs. For the time series data before the SSE, the linear trend obtained in Eq. (1) was added.

2.2 Analysis of the strain field

The strain field was calculated from the displacement field obtained by the method described in this section. The method of Shen et al. (1996) was applied to calculate the strain field. To obtain the strain field, it is necessary to uniformly and densely determine the strain values. Therefore, the strain field was calculated by placing calculation points at 0.1° intervals in a grid pattern, including the selected GNSS observation stations, and calculating the strain value at each calculation point. An outline of the calculation method for obtaining the strain field according to Shen et al. (1996) is shown as follows:

$$\begin{pmatrix} U_x^i \\ U_y^i \end{pmatrix} = \begin{pmatrix} 1 & 0 & \Delta x_i & \Delta y_i & 0 & \Delta y_i \\ 0 & 1 & 0 & \Delta x_i & \Delta y_i & -\Delta x_i \end{pmatrix} \begin{pmatrix} u_x \\ u_y \\ e_{xx} \\ e_{xy} \\ e_{yy} \\ \omega \end{pmatrix} + \begin{pmatrix} \varepsilon_x^i \\ \varepsilon_y^i \end{pmatrix} \tag{4}$$

$$E_{ij} = C_{ij} \exp\left(\frac{\Delta R_i^2 + \Delta R_j^2}{D^2}\right) \tag{5}$$

Equation (4) is an expression for the value of strain at a calculation point. x and y represent the east–west component and north–south component, respectively, with east and north taken as positive directions. i is the selected GNSS station, U_x^i and U_y^i are the displacements at the GNSS stations, Δx_i and Δy_i are the distances between GNSS stations and calculation points, u_x and u_y are the displacements at the calculation points, ω is the rigid body rotation, and e_{xx}, e_{xy} and e_{yy} are the strains at the calculation point to be obtained. e_{xx} and e_{yy} are the normal strains, and e_{xy} are the shear strains. The covariance matrix of ε_x^i and ε_y^i is expressed by E_{ij} of Eq. (5). In Eq. (5), i, j are the i-th and j-th stations, and ΔR_i and ΔR_j are the distances from the i-th and j-th stations to a certain calculation point, respectively. C_{ij} is the covariance matrix of the observation error from the calculation of the displacements at the GNSS stations. D represents the distance decaying constant, and for any SSE that was analysed in this study, D was assumed to be 17.5 km. D must include at least three GNSS stations in its range for the strain field calculation. Therefore, if the value of D was set too small, it cannot contain three or more GNSS stations, and the strain field cannot be calculated. Conversely, if the value of D was set too large, it would include more GNSS stations than necessary, and the calculated strain field will be considerably smoothed. Considering these points, we searched for the optimal value of D at intervals of 0.5, resulting in a D value of 17.5. Displacement data from GNSS stations that were within a radius of $2D$ from each calculation point were applied to obtain the strain values. Shen et al. (1996) used the equations to obtain the strain rate, whereas in this study, the total strain accumulation for each analysis period and the amount of change during the SSE occurrence were determined (Kawabata and Yoshioka 2023).

Using the strain values (e_{xx}, e_{yy}, e_{xy}) obtained above, three types of strain were calculated: dilatation, maximum shear strain, and principal strain (e.g. Sagiya et al. 2000). The equation for calculating each strain is expressed as follows:

$$e_d = e_{xx} + e_{yy} \tag{6}$$

$$e_s = \sqrt{\frac{(e_{xx} - e_{yy})^2}{4} + e_{xy}^2} \tag{7}$$

$$e_{1,2} = (e_d \pm e_s)/2 \tag{8}$$

Equations (6) and (7) are employed to determine dilatation e_d and maximum shear strain e_s, respectively. The dilatation is the strain that represents the increase in area or decrease in area at a calculation point, with a positive value indicating expansion and a negative value indicating contraction. The maximum shear strain describes the degree of lateral displacement deformation and varies in magnitude, depending on the axis taken, but the maximum value is obtained. From the values of dilatation and maximum shear strain, the principal strains e_1 and e_2 are obtained using Eq. (8). Principal strain is the strain expressed in terms of the strain in two principal axes, and the direction of the principal axes θ is obtained by Eq. (9).

$$\theta = \frac{1}{2} \tan^{-1}\left(\frac{2e_{xy}}{e_{xx} - e_{yy}}\right) \tag{9}$$

where θ is the azimuth of e_2, with north as the reference azimuth 0°, and positive clockwise. Although the maximum shear strain originally takes only positive values, in this study, we redefine the maximum shear strain to take negative values, following Kawabata and Yoshioka (2023), to investigate the relationship between strain accumulation and release. From the two principal strains $e_{1,2}$, when $|e_1| \geq |e_2|$,

$$e_s = e_1 - e_2 \tag{10}$$

and when $|e_1| < |e_2|$,

$$e_s = e_2 - e_1 \tag{11}$$

Equation (10) represents the maximum shear strain, which is positive, at the calculation point where the tensile component of the principal strain is dominant. On the other hand, Eq. (11) represents the maximum shear strain, which is negative, at the calculation point where the compressive component of the principal strain is dominant. If one only considers the magnitude of the maximum shear strain, then one should focus on its absolute value. The above three types of strains were calculated for the periods before and during each SSE, and the magnitude and spatial distribution of strain accumulation and those of strain release were compared.

3 Results

In this section, we present the analysis results of the three targeted SSEs. Following Kawabata and Yoshioka (2023), correlation coefficients were calculated for the amount of strain accumulated before an SSE and the amount of strain released during the SSE for dilatation and maximum shear strain. The correlation coefficients were calculated by extracting calculation points where the amount of displacement at the calculation point at the time of the SSE exceeded a certain threshold value (Table 3). The threshold values for each SSE were obtained by the trial-and-error method so that the negative correlation for dilatation, which represents the accumulation and release of strain, can be large. The results show that for both dilatation and maximum shear strain, the stronger the negative correlation is, the stronger the tendency for the amount of strain accumulation to be greater in the SSE area than in the surrounding areas and for the amount of strain release to be greater at the time of the SSE. This finding indicates a stronger relationship between strain accumulation and release.

Table 3 Threshold of displacement at the calculation point for each SSE

SSE (actual period)	Threshold (cm)
Tokai L-SSE (1 January 2013–5 February 2016)	2.0
Boso-Oki S-SSE (5 June 2018–20 June 2018)	1.4
Central Shikoku L-SSE (1 January 2019–31 December 2021)	0.6

3.1 2013–2016 Tokai L-SSE

The displacement, dilatation, maximum shear strain, and principal strain for the 2013–2016 Tokai L-SSE are shown in Fig. 3a–d for the period before the L-SSE and in Fig. 3e–h during the L-SSE. The displacement shows that before the L-SSE, the displacement field was uniformly oriented in the west–northwest direction due to the removal of the postseismic deformation associated with the 2011 Tohoku-Oki earthquake, which is consistent with the direction of steady displacement in the same area by Sagiya et al. (2000) (Fig. 3a). During the L-SSE, the displacement field in the southeast direction on the west side and in the east direction on the east side was identified as bordering Lake Hamana, which is consistent with the analysis results of Ozawa et al. (2016) (Fig. 3e). The maximum displacement was approximately 2.8 cm.

The dilatation shows an overall contraction before the L-SSE. The contraction was stronger along the coast and east of Lake Hamana. However, we found no particularly strong contraction at the surface above the focal region of the L-SSE (Fig. 3b). During the L-SSE, a characteristic expansion was identified mainly in Lake Hamana, and strain release attributed to the L-SSE was well confirmed (Fig. 3f). The maximum amount of strain release was 4.9×10^{-7}.

The maximum shear strain is large on the east side of Lake Hamana, with larger absolute values both before and during the L-SSE (Fig. 3c and g). In the area of strain release during the L-SSE, the release of strain is greater on the east side of Lake Hamana. This finding suggests that a spatial misalignment in dilatation and maximum shear strain occurred during the respective strain releases associated with the L-SSE.

For the principal strain, the compression in the northwest–southeast direction was generally identified before the L-SSE (Fig. 3d), while extension in the north–northwest-south–southeast direction was observed in the western area of Lake Hamana during the L-SSE (Fig. 3h). A comparison of the amount of strain accumulated before the L-SSE with the amount of strain released during the L-SSE indicates that the overall amount of strain released during the L-SSE was smaller.

Next, correlation coefficients between the amount of strain accumulated before the L-SSE and the amount of strain released during the L-SSE were calculated for dilatation and maximum shear strain (Fig. 4a and b).

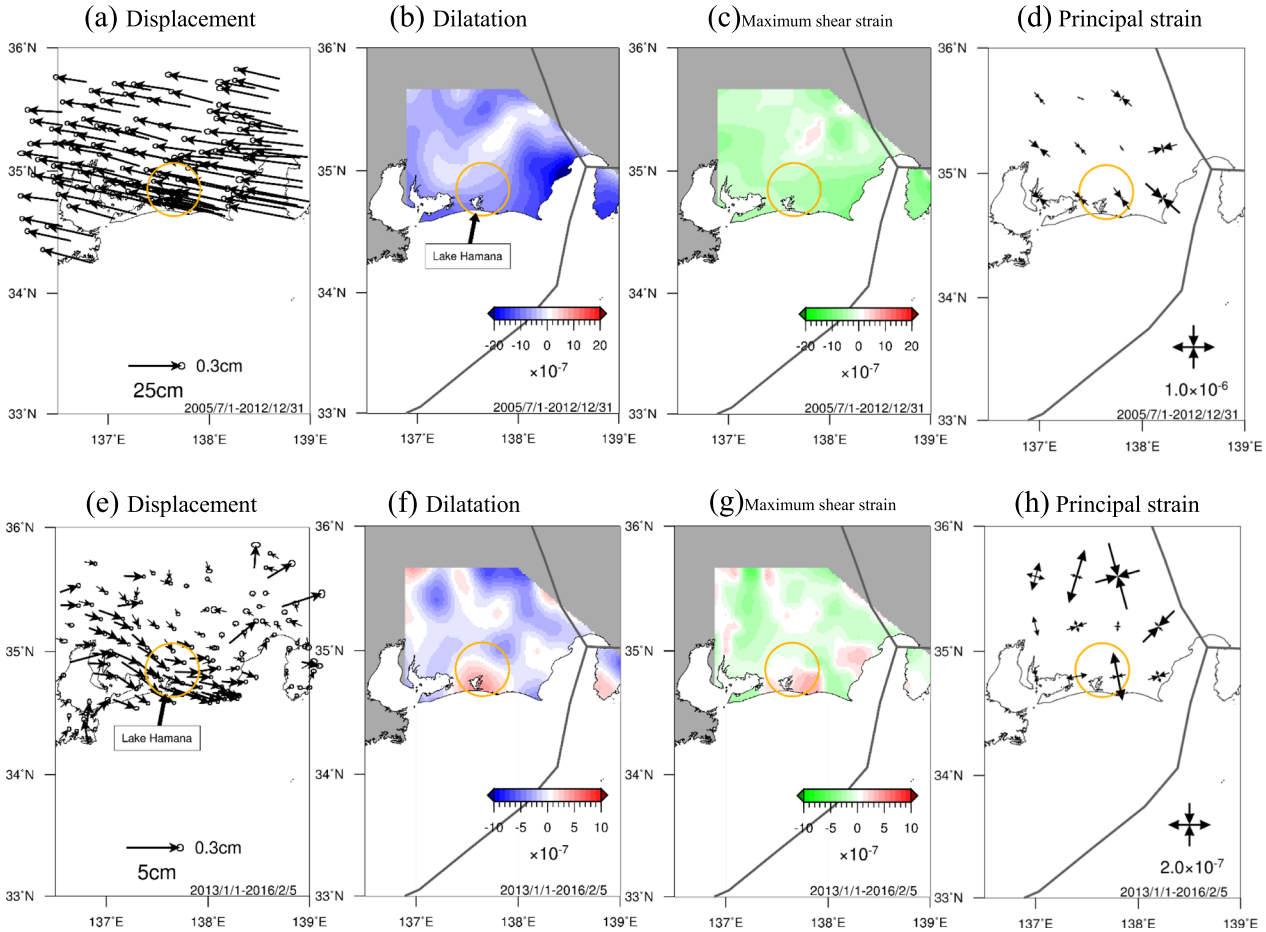

Fig. 3 Spatial distributions of displacement and each strain for the 2013–2016 Tokai L-SSE. **a**–**d** represent before the L-SSE, and **e**–**h** represent during the L-SSE. **a**, **e** Spatial distributions of displacements. The black arrows represent the displacements during the analysis period with respect to the reference station. The ellipse at the tip of each black arrow represents the error of 1σ. The orange circle denotes the approximate location of the L-SSE. **b**, **f** Spatial distributions of dilatation. The blue areas and red areas represent contraction and expansion, respectively. The thick grey line represents the plate boundary at the earth's surface (Bird 2003). The orange circle represents the same information as (**a**). **c**, **g** Spatial distributions of maximum shear strain. The green areas and red areas represent compressional regions and extensional regions, respectively. The grey lines and orange circle indicate the same information as (**b**). **d**, **h** Spatial distributions of principal strain expressed by double-headed arrows. The black outwards arrows and black inwards arrows represent extension and compression, respectively. The grey lines and orange circle represent the same information as (**b**)

Twenty-one calculation points were used to calculate the correlation coefficient, and points with a minimum displacement of 2.0 cm at the time of the L-SSE were utilized (Fig. 2a). For dilatation, the correlation coefficient was −0.70, confirming a strong negative correlation. On the other hand, the correlation coefficient for the maximum shear strain was −0.16, showing almost no negative correlation. In conclusion, the 2013–2016 Tokai L-SSE has a strong negative correlation with dilatation.

3.2 2018 Boso-Oki S-SSE

The displacement, dilatation, maximum shear strain, and principal strain associated with the 2018 Boso-Oki S-SSE are shown in Fig. 5a–d for the period before the S-SSE and in Fig. 5e–h for the period of the S-SSE occurrence. Regarding the displacement field, the northern part of the Boso Peninsula showed southwest-westward displacement, whereas the southern part of the Boso Peninsula showed northwestward displacement, with the displacement being larger in the southern part (Fig. 5a). During the S-SSE occurrence, pronounced southeastward displacement was observed in the area of the S-SSE, with a maximum displacement of approximately 3.8 cm (Fig. 5b).

For dilatation, contraction is identified before the S-SSE (Fig. 5b) and changes to expansion during the S-SSE (Fig. 5f) over the entire Boso Peninsula. In

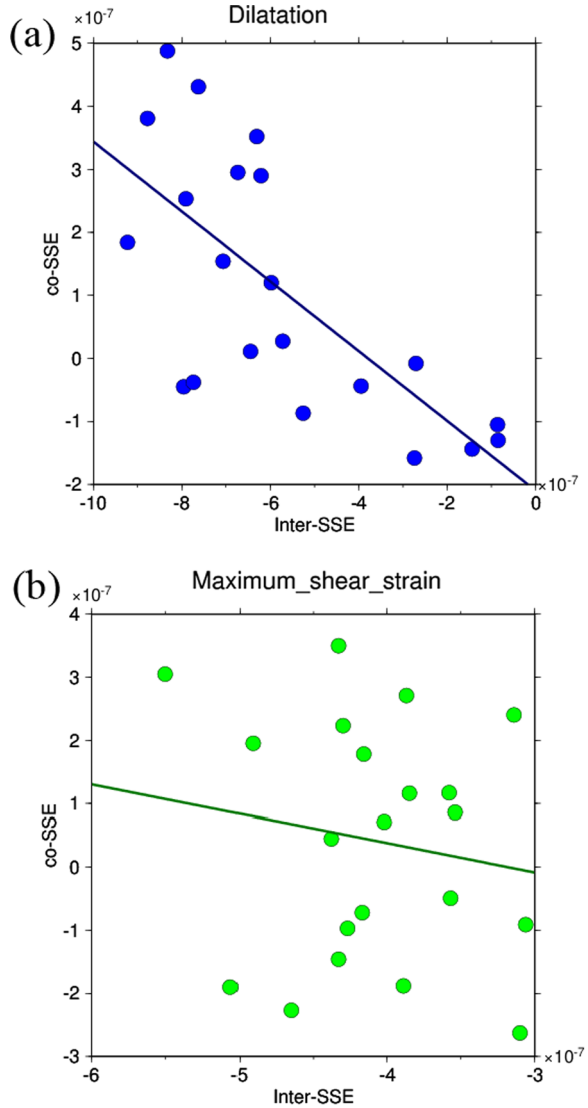

Fig. 4 Correlation diagram for the 2013–2016 Tokai L-SSE. The values of strain at the calculation points shown in Fig. 2a are plotted. The horizontal axis represents the amount of strain accumulated before the L-SSE, the vertical axis denotes the amount of strain change during the L-SSE, and the straight line is the regression line. **a** Dilatation; **b** Maximum shear strain

particular, contraction before the S-SSE and expansion during the S-SSE are observed along the eastern coast of the Boso Peninsula. The maximum amount of strain release was 7.7×10^{-7}.

Results similar to the dilatation were obtained for the maximum shear strain: both before and during the S-SSE, the absolute values were larger near the S-SSE region, and the strain release was also well confirmed (Fig. 5c and g).

With regard to principal strain, compression in the north–south direction was identified before the S-SSE (Fig. 5d), and tension in the east-west to southeast-northwest direction was observed during the S-SSE (Fig. 5h). A comparison of the amount of strain accumulation before the S-SSE with the amount of strain release during the S-SSE reveals that the amount of strain release during S-SSE occurrence was smaller.

Then, the correlation coefficients were calculated (Fig. 6a and b). Nine calculation points were used to calculate the correlation coefficients. The figure shows the points with a minimum displacement of 1.4 cm at the time of the S-SSE (Fig. 2b). The calculated values for each correlation coefficient were −0.62 for dilatation and −0.65 for maximum shear strain. These results indicate that the 2018 Boso-Oki S-SSE has a strong negative correlation for both dilatation and maximum shear strain.

3.3 2019–2021 Central Shikoku L-SSE

The displacement, dilatation, maximum shear strain, and principal strain for the 2019–2021 Central Shikoku L-SSE are shown in Fig. 7a–d for the period before the L-SSE and in Fig. 7e–h for the period of the L-SSE occurrence. Before the occurrence of the L-SSE, displacements at all stations were oriented in the northwest direction, and the amount of displacement tended to be particularly large in the south (Fig. 7a). This finding reflects the subduction of the Philippine Sea plate (Fig. 1). During the L-SSE, southeastward displacement was observed in the L-SSE area (Fig. 7e). In addition, a pronounced southeast-east displacement was observed in the southwestern part of Shikoku, which was caused by the Bungo Channel L-SSE that occurred during the same period (Ozawa et al. 2020; Seshimo and Yoshioka 2022). The maximum value of displacement was approximately 1.6 cm.

With regard to the dilatation, a large contraction was identified around the L-SSE area before the L-SSE (Fig. 7b), and a large expansion was observed around the same area during the L-SSE (Fig. 7f). The maximum strain change during the L-SSE was 8.5×10^{-7}.

No characteristic distribution of maximum shear strain was observed before the L-SSE (Fig. 7c), but during the L-SSE, a large maximum shear strain was identified along the southern coast around the L-SSE area (Fig. 7g).

For the principal strain, compression in the northwest–southeast direction was dominant before the L-SSE (Fig. 7d), but during the L-SSE, north–south to northwest-southeast tension was observed in the L-SSE area (Fig. 7h). A comparison of the amount of strain accumulated before the L-SSE with the amount of strain released during the L-SSE indicates that the amount of strain released during the L-SSE was smaller.

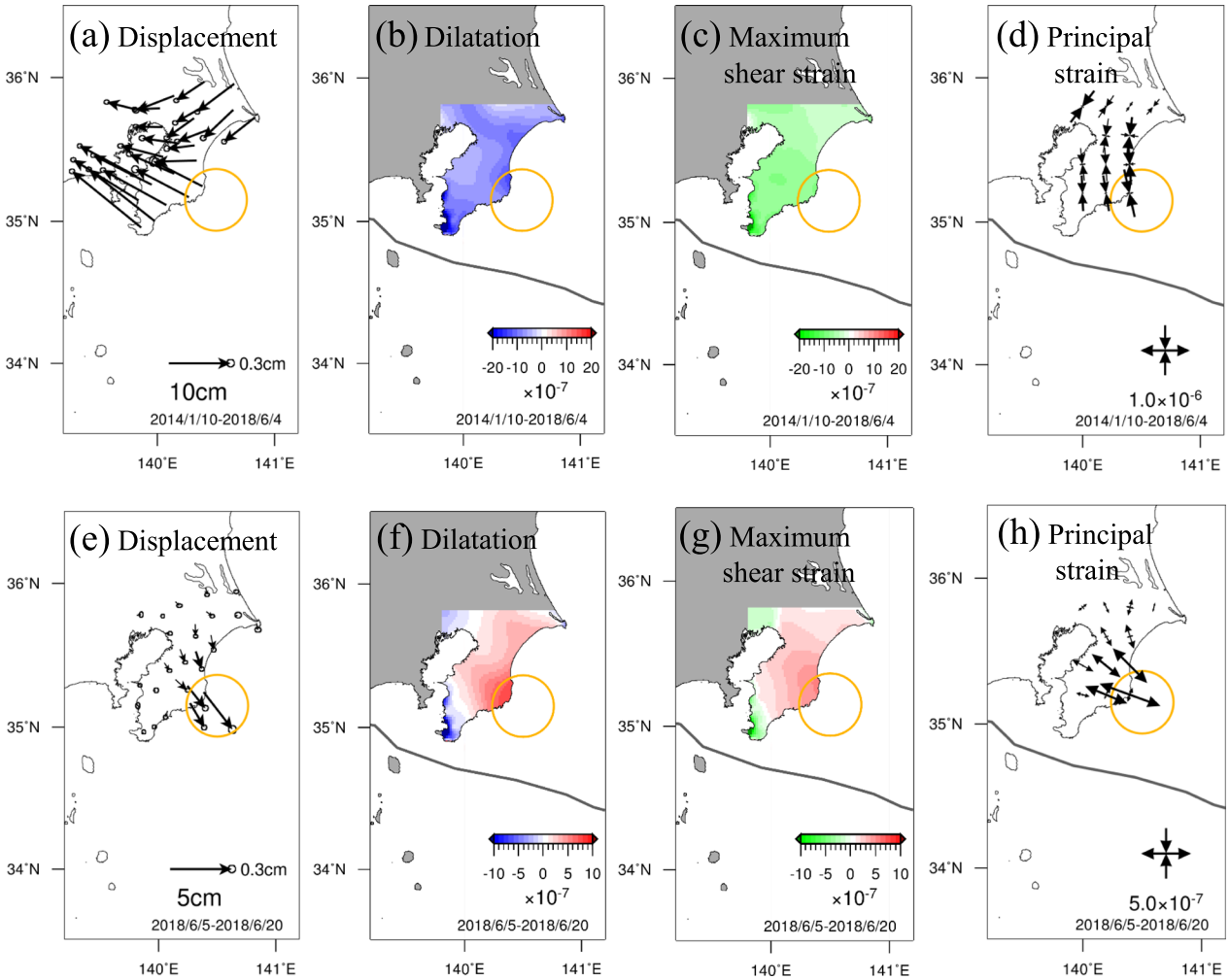

Fig. 5 Spatial distributions of displacement and each strain for the 2018 Boso-Oki S-SSE. The same information in Fig. 3a–h, with the exception of the 2018 Boso-Oki S-SSE, is depicted

Correlation coefficients were obtained in the same way as described above (Fig. 8a and b). Thirteen calculation points were used to calculate the correlation coefficients, and points with a minimum displacement of 0.6 cm at the time of the L-SSE were selected (Fig. 2c). The correlation coefficients were calculated to be −0.76 for dilatation and 0.10 for maximum shear strain, indicating a strong negative correlation for dilatation.

4 Discussion

4.1 Relationship between accumulated strain and strain released by the SSE

For the 2013–2016 Tokai L-SSE, a strong negative correlation was identified in the dilatation. This finding indicates that in the vicinity of Lake Hamana, where the L-SSE signal was detected, the greater the amount of strain accumulated prior to the L-SSE, the stronger the tendency for greater strain release during the L-SSE. However, even stronger contraction is observed on the east side of Lake Hamana (Fig. 3b), which is included in the assumed source region of the Tokai earthquake (CDMC 2001), a megathrust earthquake, for which the possibility of another occurrence in the near future has been pointed out. The stronger contraction on the east side is considered associated with more strain accumulation towards the occurrence of the Tokai earthquake. Therefore, there is a possibility that the accumulation of strain in the vicinity of Lake Hamana, where the L-SSE occurs, has been obscured by the accumulation of strain in the assumed source region. In Fig. 4a, there are several calculation points that show contraction at the time of the L-SSE, despite the strong negative correlation. This may be contraction relative to expansion due to the release of strain around Lake Hamana associated with the L-SSE.

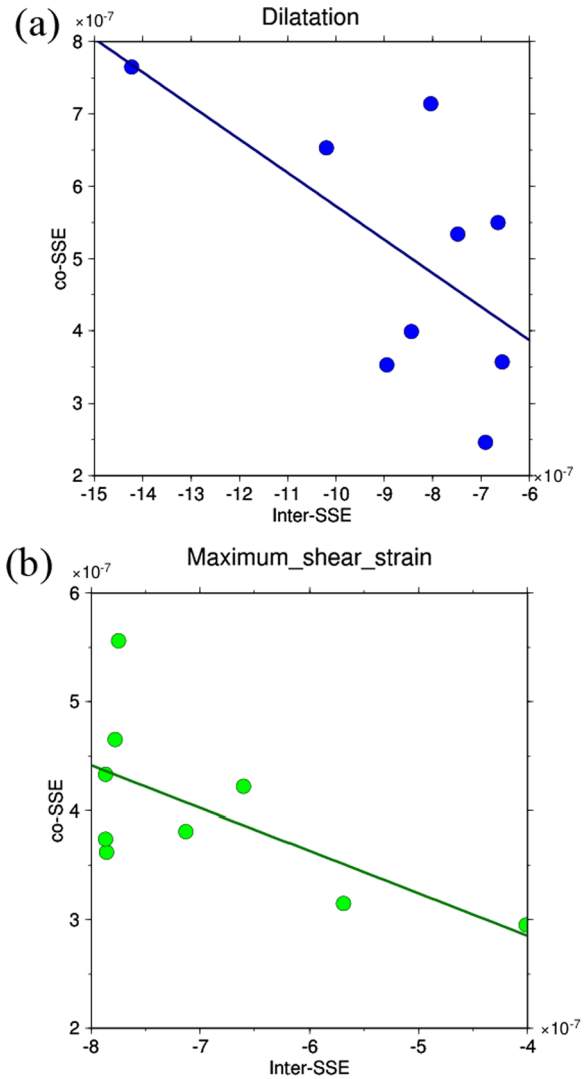

Fig. 6 Correlation diagram for the 2018 Boso-Oki S-SSE. The values of strain at the calculation points shown in Fig. 2b are plotted. The same information in Fig. 4a and b, with the exception of the 2018 Boso-Oki S-SSE, is depicted

In the 2018 Boso-Oki S-SSE, the amount of accumulated strain before the S-SSE and the amount of released strain at the time of the S-SSE were larger in the area surrounding the S-SSE region for both dilatation and maximum shear strain, suggesting that more strain accumulated before the S-SSE was released by the S-SSE than in the surrounding area (Fig. 5b, c, f and g). The correlation coefficients in Fig. 6a and b were also negative, indicating that both the dilatation and maximum shear strain of the Boso-Oki S-SSE were caused by the accumulation of a larger amount of strain than in the surrounding area and that the strain was largely released during the S-SSE. The large negative correlation of maximum shear strain indicated that lateral deformation was predominant in the 2018 Boso-Oki S-SSE occurrence region, both during the strain accumulation and release periods, and that there was an opposite relationship between the two. It should be noted that the calculation of the maximum shear strain does not consider the direction of the strain. Therefore, the correlation coefficient of the maximum shear strain and the direction of the principal strain should be separately considered. For a discussion of the principal strain field, see the Additional file 1: Text A1. Thus, there was a strong relationship between strain accumulation and strain release.

For the 2019–2021 Central Shikoku L-SSE, dilatation showed a strong negative correlation (Fig. 8a), as the accumulation of strain prior to the L-SSE and the release of strain during the L-SSE were well identified in the area surrounding the L-SSE area (Fig. 7b and f). On the other hand, for maximum shear strain, the negative correlation was not strong (Fig. 8b) as no characteristic spatial pattern of strain was identified in the L-SSE region prior to the L-SSE (Fig. 7c and g). These results indicate that in the 2019–2021 Central Shikoku L-SSE, there is a large accumulation of dilatation due to contraction before the L-SSE and a large expansion due to the release of strain during the L-SSE.

4.2 Estimation of the number of years of strain accumulation and the strain release rate

The correlation coefficient values obtained for each SSE in Sect. 3 demonstrated that there is a strong relationship between accumulation and release in dilatation for the 2013–2016 Tokai L-SSE and the 2019–2021 Central Shikoku L-SSE and that there is a strong relationship between accumulation and release in both dilatation and maximum shear strain for the 2018 Boso-Oki S-SSE. In this section, we attempt to calculate "the number of years of strain accumulation" using the method proposed by Kawabata and Yoshioka (2023) for these strains, for which the negative correlation was particularly strong.

The number of years of strain accumulation T was defined as the number of years required to accumulate an amount of strain equivalent to the amount of strain released by each SSE and was estimated by the following two equations:

$$\mathrm{RMS} = \sqrt{\frac{\sum_{i=1}^{n}\left(\left|e_i^{\mathrm{SSE}}\right| - c|e_i|\right)^2}{n}} \tag{12}$$

$$T = cT_0 \tag{13}$$

where n in Eq. (12) represents the number of calculation points and the same points were used to obtain the value of the correlation coefficient. e_i^{SSE} is the amount of strain

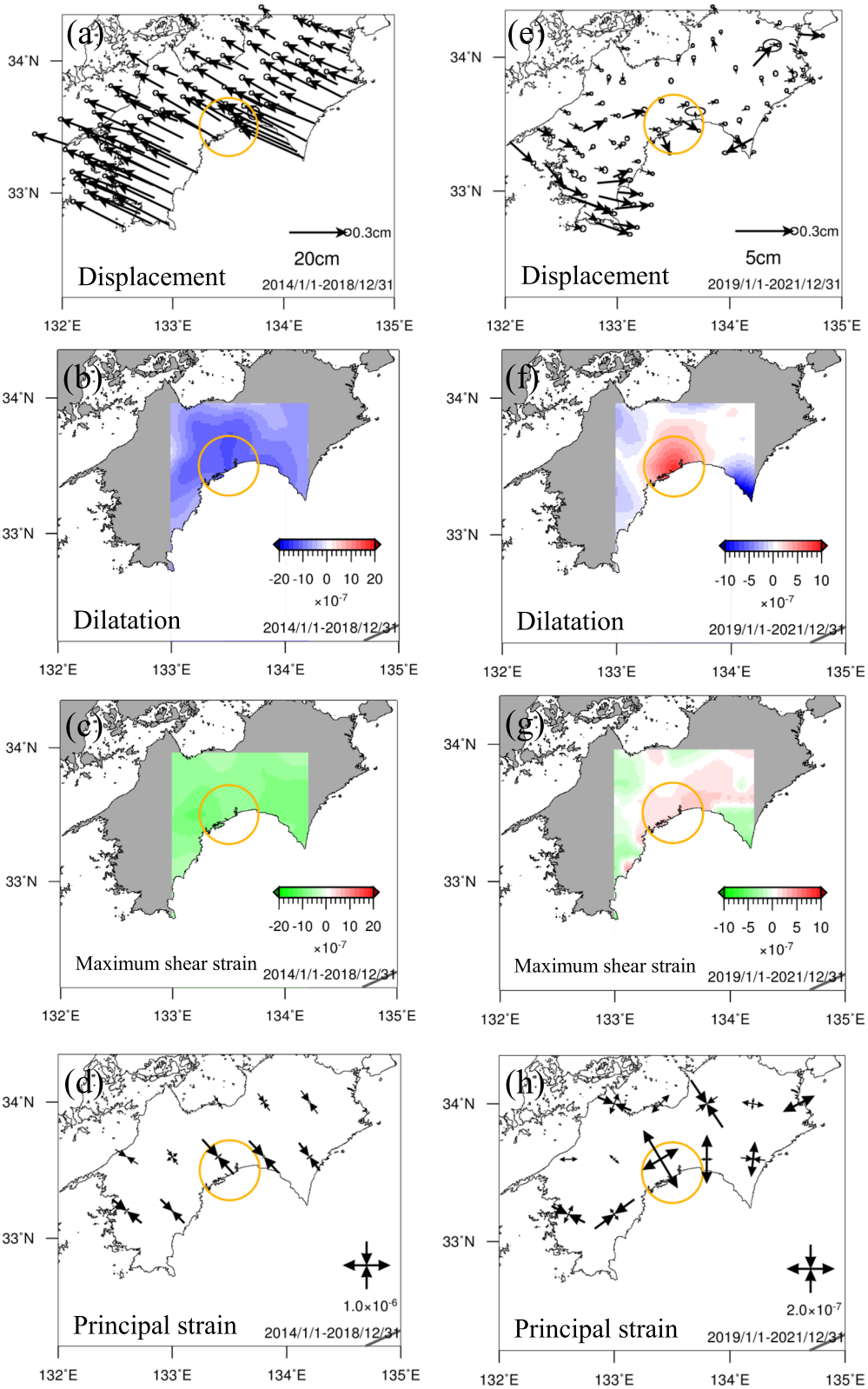

Fig. 7 Spatial distributions of displacement and each strain for the 2019–2021 Central Shikoku L-SSE. The same information in Fig. 3a–h, with the exception of the 2019–2021 Central Shikoku L-SSE, is depicted

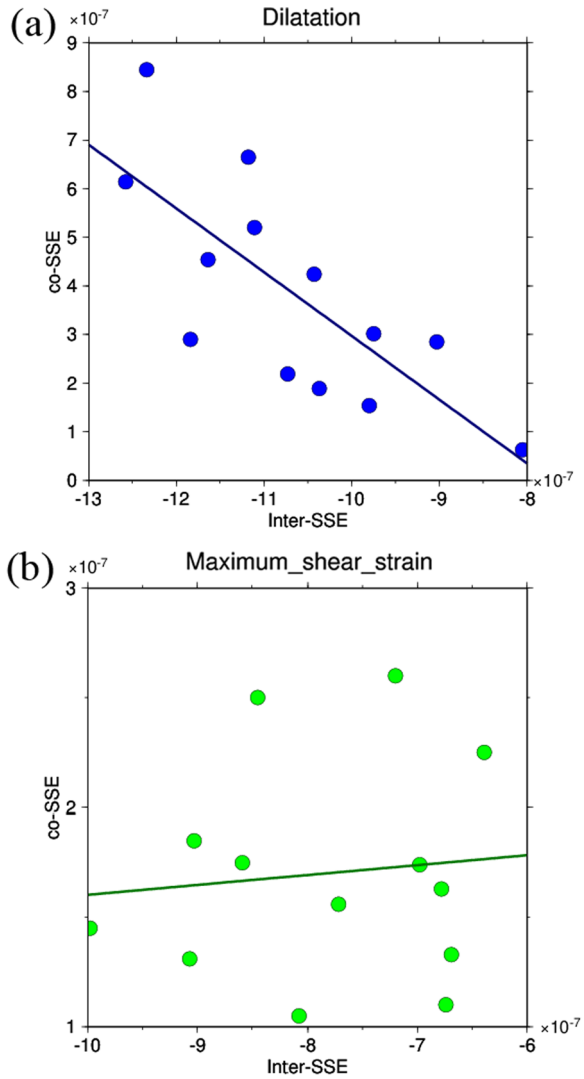

Fig. 8 Correlation diagram for the 2019–2021 Central Shikoku L-SSE. The values of strain at the calculation points shown in Fig. 2c are plotted. The same information shown in Fig. 4a and b, with the exception of the 2019–2021 Central Shikoku L-SSE, is depicted

released at the time of the SSE at the i-th calculation point, and e_i is the amount of strain accumulated at the i-th calculation point for the period before the SSE. Using the least squares method, the value of c was obtained such that the RMS value was minimized, in which c was searched at intervals of 0.01. In Eq. (13), T_0 is the period before each SSE set in this study, and the accumulated year T was obtained by taking the product of the value of c when the RMS value was minimized in Eq. (12).

In Table 4, we show the estimated number of years of accumulation of strains that were strongly negatively correlated in each SSE. For the 2013–2016 Tokai L-SSE and the 2019–2021 Central Shikoku L-SSE, the number of accumulation years was 2.3 and 1.9, respectively. For the dilatation and maximum shear strain of the 2018 Boso-Oki S-SSE, the number of accumulation years was 2.6 and 2.5, respectively, which were similar. Considering that the periods before these SSEs were 7.5, 5.0, and 4.4 years, respectively, the accumulation years were approximately 30%, 40%, and 60% for the 2013–2016 Tokai L-SSE, the 2019–2021 Central Shikoku L-SSE, and the 2018 Boso-Oki S-SSE, respectively. This finding implied that each of these percentages of strain accumulated prior to each SSE was released by each SSE. In this study, the ratio of strain release to strain accumulation was calculated for the three SSEs. However, direct comparisons were difficult to conduct due to the difference in each SSE occurrence region for the analysed GNSS station locations and the density of these stations. For example, the Tokai L-SSE occurred just below the land area and was covered widely by the GNSS stations. However, the Boso-Oki S-SSE occurred in an offshore area and was not well covered by land-based GNSS stations. Therefore, in the following discussion, we do not directly compare the ratio of strain release to accumulation of strain but will discuss each SSE individually in more detail.

Table 4 Years of strain accumulation for each SSE

SSE (duration)	Estimated years of dilatation accumulation *T* (Analysis period prior to the SSE) (year)	Estimated years of maximum shear strain accumulation *T* (Analysis period prior to the SSE) (year)	The percentage of strain release for dilatation accumulation (%)	The percentage of strain release for maximum shear strain accumulation (%)
Tokai L-SSE (1 January 2013–5 February 2016)	2.3 (7.5)		31	
Boso-Oki S-SSE (5 June 2018–20 June 2018)	2.6 (4.4)	2.5 (4.4)	59	57
Central Shikoku L-SSE (1 January 2019–31 December 2021)	1.9 (5.0)		38	

The values in parentheses indicate the analysis period before the SSEs in this study, and the values without parentheses indicate the accumulation years *T* calculated by the above method

Regarding the 2013–2016 Tokai L-SSE, prior to this L-SSE, L-SSEs had occurred in the same region from 2000 to 2005 (e.g. Miyazaki et al. 2006). Kawabata and Yoshioka (2023) analysed the L-SSE and stated that approximately 50% of the strain was released by the L-SSE. Although the results of the present study are smaller than those obtained by Kawabata and Yoshioka (2023), they indicated that the GNSS could not capture Tokai L-SSEs, which would have occurred before 2000, as the GNSS started observing crustal deformation in 1996. Therefore, based on past studies of crustal deformation in the Tokai region, the accumulation period was estimated by assuming that the accumulation period before the L-SSE was approximately 10 years. Therefore, uncertainty remains in the estimation of the accumulation year in the study. However, for the SSEs in other regions in Kawabata and Yoshioka (2023) (Bungo Channel L-SSE in 2009–2011 and 2018–2019 and Boso-Oki S-SSE in 2007), the timing of the previous SSEs could be identified from the analysis of GNSS data, so the SSE period prior to occurrence could be accurately determined. As a result, there was a release of approximately 30% of the strain for the three SSEs. This result is consistent with the result of the accumulation year of the 2013–2016 Tokai L-SSE estimated in this study, and the result of approximately 30% strain release for the amount of strain accumulation by the 2013–2016 Tokai L-SSE is a reasonable value.

The 2019–2021 Central Shikoku L-SSE had a strain release of approximately 40%. This finding may have been related to the smaller magnitude of a Central Shikoku L-SSE that occurred prior to the 2019–2021 Central Shikoku L-SSE. Crustal deformations similar to the L-SSE have been observed in this region in 1977–1980 (Kobayashi 2012) and 2013 (JMA 2014) as well. JMA (2014) reported that an L-SSE had been occurring in Central Shikoku for approximately one year since early 2013. However, this L-SSE had a relatively short duration, and the amount of displacement at the Earth's surface was less than 1 cm, indicating that it may have been a small L-SSE. Based on these data, the strain release by the 2013 L-SSE was considered quite small. Therefore, it could be interpreted that the 2019–2021 L-SSE that was targeted in this study released strains, including strains that were not released in the previous L-SSE. For the 30% value of the Tokai L-SSE and 40% value of the Central Shikoku L-SSE, as in the interpretation by Kawabata and Yoshioka (2023), the accumulation of strain was considered to have an effect not only on the L-SSE occurrence area but also on the shallower areas where a megathrust earthquake will occur in the future.

For the 2018 Boso-Oki S-SSE, the amount of released strain was approximately 60% of the amount of strain accumulated, which is larger than the 30% value of reported by Kawabata and Yoshioka (2023) for the 2007 Boso-Oki S-SSE. Since the 60% value for the Boso-Oki S-SSE was significantly larger than the values for the other two SSEs in this study and the four SSEs analysed by Kawabata and Yoshioka (2023), we compared it to a previous S-SSE that occurred in the same region (the 2007 Boso-Oki S-SSE) to investigate whether this was due to regional characteristics or to the specificity of this event. As a result, this difference may have been attributed to the influence of the earthquake swarms that occurred in the Boso Peninsula at the time of the S-SSE. On the Boso Peninsula, earthquake swarms were prevalent, mainly on the deep side of the S-SSE region at the plate boundary, at approximately the same time as the past Boso-Oki S-SSE (Ozawa et al. 2007). Therefore, it is possible that some of the strain that was not released by the S-SSE was released by these earthquake swarms. Here, we investigated the number of earthquakes that occurred in the vicinity of the S-SSE area in the same period as the Boso-Oki S-SSEs in 2007 and 2018. In Fig. 9a and b, we plotted the epicentres of the earthquakes that were reported in the unified hypocentre catalogue of the Japan Meteorological Agency (JMA) as having a magnitude of 4.0 or greater, which were considered to be associated with each S-SSE. The results showed that 16 earthquakes occurred in the 2007 Boso-Oki S-SSE, while only 4 earthquakes occurred in the 2018 Boso-Oki S-SSE. Note that these earthquakes were not detected as coseismic steps in the GNSS time series data because they had JMA magnitudes of less than 6. This finding suggests that in the 2007 Boso-Oki S-SSE, there was less strain released by the S-SSE, but that the remaining strain was released by many earthquake swarms. On the other hand, in the 2018 Boso-Oki S-SSE analysed in this study, there was more strain release by the S-SSE and less strain release by earthquake swarms.

5 Conclusions

In this study, using GNSS time series data, we analysed the strain fields before and during the 2013–2016 Tokai L-SSE, the 2018 Boso-Oki S-SSE, and the 2019–2021 Central Shikoku L-SSE in terms of the spatial distribution and magnitude relationships. The significant results obtained in this study are summarized as follows:

1. With respect to the dilatation of the 2019–2021 Central Shikoku L-SSE and the dilatation and maximum shear strain of the 2018 Boso-Oki S-SSE, the area where the SSE occurred showed greater accumulation and release of strain before and during the SSE than the surrounding area at the earth's surface.

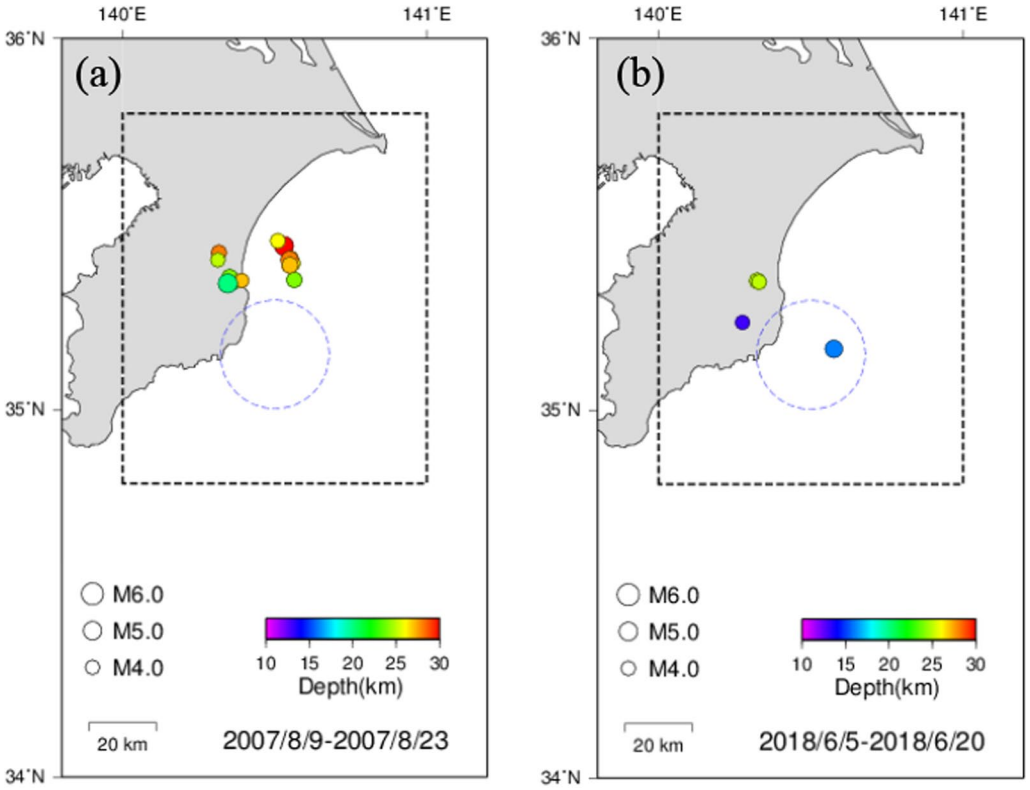

Fig. 9 Earthquakes that occurred near the Boso Peninsula with JMA magnitude 4.0 or greater at the time of the Boso-Oki S-SSEs are plotted. The colour solid circles represent the epicentres of the earthquakes that occurred at depths shallower than 30 km determined by the JMA, and the colour of the circle indicates the depth of the earthquake. The blue dashed circle indicates the approximate location of the Boso-Oki S-SSE. The black dashed line represents the search area for the earthquakes, whose spatial range is 34.8°–35.8° N and 140.0°–141.0° E. **a** 2007 Boso-Oki S-SSE. The period of the plotted earthquake is from 9 August 2007 to 23 August 2007. **b** 2018 Boso-Oki S-SSE. The period of the plotted earthquake is from 5 June 2018 to 20 June 2018

2. For the 2013–2016 Tokai L-SSE, the accumulation of strain before the L-SSE around Lake Hamana is difficult to detect due to the accumulation of larger strain in the assumed source region of a possible future Tokai earthquake on the plate boundary. However, since a strong negative correlation in dilatation was identified, the greater the accumulation of strain is prior to the occurrence of the L-SSE, the stronger the tendency for a greater release of strain at the time of the L-SSE.
3. Approximately 30% of the accumulated strain was released for the 2013–2016 Tokai L-SSE. The values are consistent with those estimated for the 2007 Boso-Oki S-SSE and the 2009–2010 and 2018–2019 Bungo Channel L-SSEs in the previous study, for which the period prior to the SSEs is known.
4. Approximately 40% of the accumulated strain was released for the 2019–2021 Central Shikoku L-SSE. The value is considered to have a slightly larger ratio of the amount of strain released as the previous L-SSE occurred in 2013 which was smaller than the 2019–2021 L-SSE targeted in this study. Therefore, the release of strain from the 2019–2021 L-SSE is considered to have included strain that was not released last time, resulting in a slightly larger ratio of the amount of released strain.
5. Approximately 60% of the accumulated strain was released for the 2018 Boso-Oki S-SSE. The larger value compared to the results of the previous study can be attributed to the occurrence of fewer earthquake swarms. There were fewer earthquake swarms during the 2018 Boso-Oki S-SSE than during the 2007 Boso-Oki S-SSE occurrence. Therefore, it can be considered that the 2018 S-SSE released more of the strain that was not released by the earthquake swarms.

Abbreviations

CDMC	Central Disaster Management Council
GNSS	Global Navigation Satellite System
GSI	Geospatial Information Authority of Japan
JMA	Japan Meteorological Agency
L-SSE	Long-term slow slip event
SSE	Slow slip event
S-SSE	Short-term slow slip event

Supplementary Information

The online version contains supplementary material available at https://doi.org/10.1186/s40645-023-00557-z.

Additional file 1. Text A1. The principal strain field between the accumulation and release periods for the 2018 Boso-Oki S–SSE. **Table A1.** Fault parameters for the three rectangular faults shown in Fig. A1. **Figure A1.** Observed and calculated displacement, principal strain rate, and principal strain fields related to the 2018 Boso-Oki S-SSE. Reference.

Acknowledgements

We thank the Editor, Y. Yagi and two anonymous reviewers for their constructive comments to improve our manuscript. In this study, we utilized the daily coordinate data of GNSS stations provided by the GSI (https://www.gsi.go.jp/ENGLISH/geonet_english.html), the electronic reference point maintenance work list (https://terras.gsi.go.jp/denshi_hosyu.php), JMA's seismic intensity database (https://www.data.jma.go.jp/svd/eqdb/data/shindo/index.html), and JMA unified hypocentre catalogue (https://www.data.jma.go.jp/eqev/data/daily_map/index.html). Figures were created using Generic Mapping Tools (version: GMT 3.4.6, URL link: https://www.generic-mapping-tools.org/download/) by Wessel and Smith (1998).

Author contributions

HK analysed GNSS time series data, calculated the strain field, and wrote the paper. SY organized and guided the study, pointed out possible problems with the study, advised about solutions, and edited the paper. FOC pointed out possible problems with the study and advised about solutions. All authors read and approved the final manuscript.

Funding

This work was partly supported by a MEXT KAKENHI grant [Grant No. 21H05203] and a Kobe University Strategic International Collaborative Research Grant (Type B Fostering Joint Research).

Availability of data and materials

In this study, we utilized the daily coordinate data of GNSS stations provided by the GSI (https://www.gsi.go.jp/ENGLISH/geonet_english.html), the electronic reference point maintenance work list (https://terras.gsi.go.jp/denshi_hosyu.php), JMA's seismic intensity database (https://www.data.jma.go.jp/svd/eqdb/data/shindo/index.html), and JMA's centralized epicentre catalogue (https://www.data.jma.go.jp/eqev/data/daily_map/index.html).

Declarations

Competing interests

The authors declare that they have no competing interests.

Received: 30 December 2022 Accepted: 28 April 2023
Published online: 08 June 2023

References

Bird P (2003) An updated digital model of plate boundaries. Geochem Geophys Geosyst 4(3):1027. https://doi.org/10.1029/2001GC000252
Central Disaster Management Council (2001) Report of special board of inquiry on Tokai earthquake. 1–8
DeMets C, Gordon RG, Argus DF (2010) Geologically current plate motions. Geophys J Int 181:1–80. https://doi.org/10.1111/j.1365-246X.2009.04491.x
Japan Meteorological Agency (2014) Baseline length changes perpendicular to the trench axes of Japan. Bull Coord Comm Earthq Predict Jpn 91:30–34
Kawabata H, Yoshioka S (2023) Strain accumulation and release processes associated with the occurrence of SSEs in the subduction zones of the Japanese Islands. Sci Rep 13:1379. https://doi.org/10.1038/s41598-023-28016-1
Kobayashi A (2010) A small scale long-term slow slip occurred in the western Shikoku in 2005. Zisin 2(63):97–100
Kobayashi A (2012) Long-term slow slip event around Kochi City from 1977 to 1980. Zisin 2(64):63–73. https://doi.org/10.4294/zisin64.63
Kobayashi A (2017) Objective detection of long-term slow slip events along the Nankai Trough using GNSS data (1996–2016). Earth Planets Space 69:171. https://doi.org/10.1186/s40623-017-0755-7
Miyazaki S, Segall P, McGuire JJ, Kato T, Hatanaka Y (2006) Spatial and temporal evolution of stress and slip rate during the 2000 Tokai slow earthquake. J Geophys Res 111:B03409. https://doi.org/10.1029/2004JB003426
Ozawa S, Murakami M, Kaidzu M, Tada T, Sagiya T, Hatanaka Y, Yarai H, Nishimura T (2002) Detection and monitoring of ongoing aseismic slip in the Tokai region, central Japan. Science. https://doi.org/10.1126/science.1076780
Ozawa S, Suito H, Tobita M (2007) Occurrence of quasi-periodic slow-slip off the east coast of Boso peninsula, Central Japan. Earth Planets Space 59:1241–1245. https://doi.org/10.1186/BF03352072
Ozawa S, Yarai H, Imakiire T, Tobita M (2013) Spatial and temporal evolution of the long-term slow slip in the Bungo Channel, Japan. Earth Planets Space 65:67–73. https://doi.org/10.5047/eps.2012.06.009
Ozawa S, Tobita M, Yarai H (2016) A possible restart of an interplate slow slip adjacent to the Tokai seismic gap in Japan. Earth Planets Space 68:54. https://doi.org/10.1186/s40623-016-0430-4
Ozawa S, Kawabata R, Kokado K, Yarai H (2020) Long-term slow slip events along the Nankai trough delayed by the 2016 Kumamoto earthquake, Japan. Earth Planets Space 72:61. https://doi.org/10.1186/s40623-020-01189-z
Sagiya T, Miyazaki S, Tada T (2000) Continuous GPS array and present-day crustal deformation of Japan. Pure Appl Geophys 157:2303–2322. https://doi.org/10.1007/PL00022507
Seshimo Y, Yoshioka S (2022) Spatiotemporal slip distributions associated with the 2018–2019 Bungo Channel long-term slow slip event inverted from GNSS data. Sci Rep 12:343. https://doi.org/10.1038/s41598-021-03982-6
Shen Z-K, Jackson DD, Ge BX (1996) Crustal deformation across and beyond the Los Angeles basin from geodetic measurements. J Geophys Res 101(B12):27957–27980. https://doi.org/10.1029/96JB02544
Tobita M (2016) Combined logarithmic and exponential function model for fitting postseismic GNSS time series after 2011 Tohoku-Oki earthquake. Earth Planets Space 68:41. https://doi.org/10.1186/s40623-016-0422-4
Wessel P, Smith WHF (1998) New, improved version of generic mapping tools released. EOS Trans Am Geophys Union 79:579. https://doi.org/10.1029/98EO00426
Yoshioka S, Matsuoka Y, Ide S (2015) Spatiotemporal slip distributions of three long-term slow slip events beneath the Bungo Channel, southwest Japan, inferred from inversion analyses of GPS data. Geophys J Int 201:1437–1455. https://doi.org/10.1093/gji/ggv022

Publisher's Note